Editors' Suggestion

Eliminating Defect States in Monolayer Tungsten Diselenide by Coupling with a c-Plane Sapphire Surface

Chen Huang,[1,*] Jinhuan Wang,[2,3,*,†] Yilin Chen,[1,*] Zuo Feng,[1] Yuexing Xia,[4,5] Guangjie Yao,[1] Mengze Zhao,[1] Guodong Xue,[1] Si Zhou,[2,3] Xiaozhi Xu,[2,3] Xinfeng Liu,[4,5] Enge Wang,[6,7] Ji Chen,[1,8,‡] Kaihui Liu,[1,8,9,§] and Hao Hong[1,8,‖]

[1]*State Key Lab for Mesoscopic Physics and Frontiers Science Center for Nano-optoelectronics, School of Physics, Peking University, Beijing, China*

[2]*Guangdong Basic Research Center of Excellence for Structure and Fundamental Interactions of Matter, Guangdong Provincial Key Laboratory of Quantum Engineering and Quantum Materials, School of Physics, South China Normal University, Guangzhou 510006, China*

[3]*Guangdong-Hong Kong Joint Laboratory of Quantum Matter, Frontier Research Institute for Physics, South China Normal University, Guangzhou 510006, China*

[4]*CAS Key Laboratory of Standardization and Measurement for Nanotechnology, National Center for Nanoscience and Technology, Beijing 100190, China*

[5]*University of Chinese Academy of Sciences, Beijing 100049, China*

[6]*International Centre for Quantum Materials, Collaborative Innovation Centre of Quantum Matter, Peking University, Beijing, China*

[7]*Tsientang Institute for Advanced Study, Zhejiang, China*

[8]*Interdisciplinary Institute of Light-Element Quantum Materials, Peking University, Beijing, China*

[9]*Songshan Lake Materials Lab, Institute of Physics, Chinese Academy of Sciences, Dongguan, China*

(Received 18 December 2024; accepted 6 August 2025; published 15 September 2025)

Semiconducting transition metal dichalcogenides are promising platforms for exploring emergent two-dimensional (2D) exciton physics and constructing 2D optoelectronic devices. However, even in mechanically exfoliated and hexagonal boron nitride encapsulated samples that are expected to maintain the most intrinsic properties, shallow defect states are still unavoidable. Here, we reported a method for eliminating the defect states in monolayer WSe_2 by coupling it with a c-plane sapphire surface. We found that the defect-relevant photoluminescence peaks at cryogenic temperatures can be completely suppressed in WSe_2 on c-plane sapphire, resulting in intrinsic exciton radiation, prolonged lifetime, and increased diffusion length. *Ab initio* calculations revealed that the surface of c-plane sapphire is much more active than other planes, where oxygen atoms preferentially transfer to WSe_2 to repair selenium vacancy defects. Our Letter provides a new platform for defect engineering, which will promote the development of high-performance electronic and optoelectronic devices based on 2D materials.

DOI: 10.1103/lswx-rxss

Transition metal dichalcogenides (TMDs, MX_2) composed of transition metal atoms ($M = \mathrm{W}, \mathrm{Mo}, \ldots$) and chalcogenide atoms ($X = \mathrm{S}, \mathrm{Se}, \ldots$) are the most prevalent semiconductors within the two-dimensional (2D) material family. The hexagonal-phase monolayer exhibits a honeycomb lattice akin to that of graphene; however, the broken inversion symmetry introduces a direct band gap at the Brillouin zone corners. Near the band gap, electron-hole pairs form tightly bound excitons owing to strong Coulomb interactions, which dominate the low-energy interband physics of TMDs [1–3]. The wave functions of the excitons are localized primarily around the middle transition metal atoms [4]. Consequently, the excitonic properties are well protected from surrounding distortions, facilitating the direct observation of complex excitonic phenomena including charged excitons (trions), biexcitons, dark excitons, Rydberg excitons, and chiral phonon replicas [5–22]. However, this protection in monolayers is still less effective. The surficial chalcogenide atoms are prone to forming vacancies due to the weak covalent bond strength (between 2.3 and 2.9 eV), leading to shallow defect-related states at the midgap [23–28]. Even in the "cleanest" mechanically exfoliated and hexagonal boron nitride hexagonal boron nitride (hBN) encapsulated devices, excitons in monolayer TMDs can be trapped by defects and exhibit defect-related photoluminescence (PL) emission at cryogenic temperatures [29,30].

Modifying the midgap defect states and mitigating the impacts of defects in TMDs are of central importance for

*These authors contributed equally to this work.
†Contact author: jinhuanwang@scnu.edu.cn
‡Contact author: ji.chen@pku.edu.cn
§Contact author: khliu@pku.edu.cn
‖Contact author: haohong@pku.edu.cn

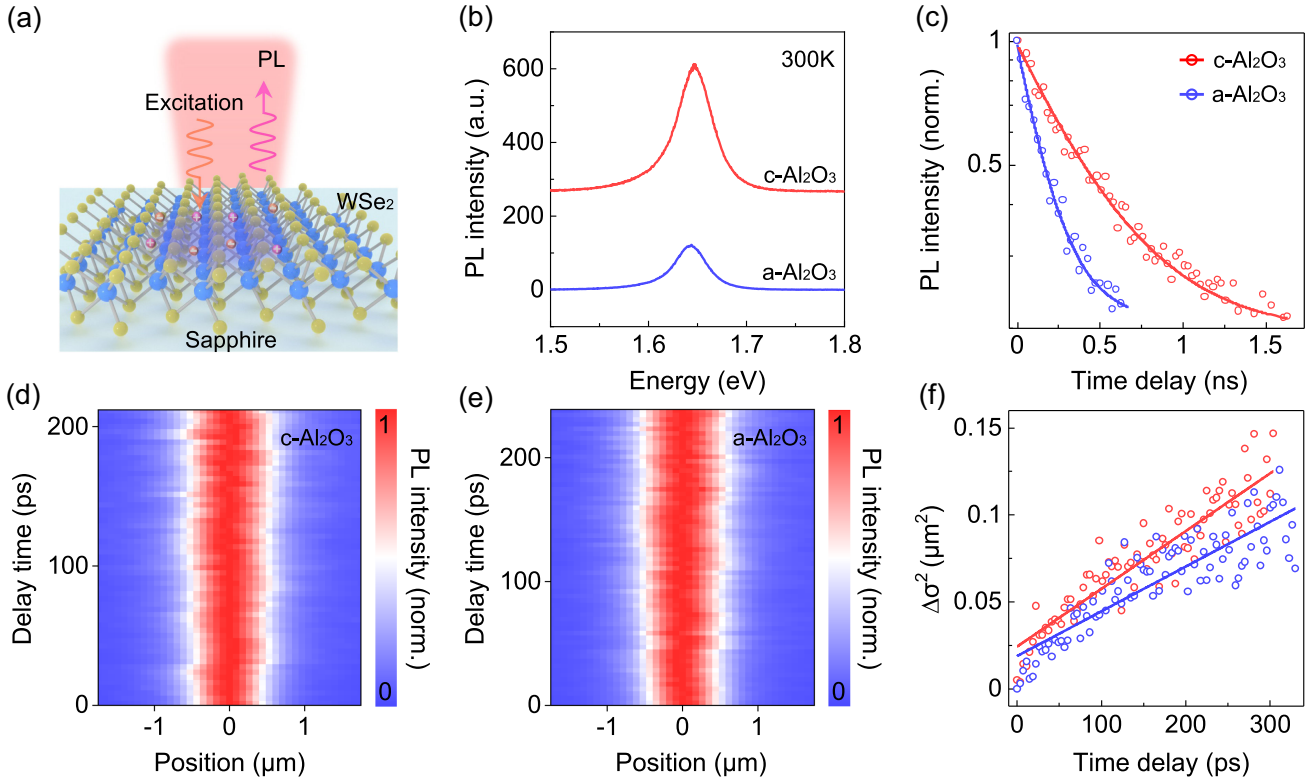

FIG. 1. PL spectra of WSe_2 monolayers on different planes of sapphire substrates. (a) Schematic diagram of the PL process with a reflective geometry measurement. (b) PL spectra of WSe_2 on c-plane and a-plane sapphire substrates. Under the same conditions, the PL intensity on the c-plane sapphire is 3 times greater than that the on a-plane sapphire. (c) Time-resolved PL spectra. The exciton lifetimes are 420 and 170 ps on c-plane and a-plane sapphire substrates, respectively. (d),(e) Normalized diffusion mappings on c-plane (d) and a-plane (e) sapphire substrates. The horizontal axis corresponds to the PL distribution, the vertical axis corresponds to the time delay after excitation, and the color indicates the normalized PL intensity. (f) Time-dependent mean-squared distribution for PL emission spot broadening. The diffusivity on the c-plane sapphire surface is greater than that on the a-plane sapphire. All experiments were conducted at room temperature.

the exploration of strongly correlated physics and potential applications in optoelectronic and electronic devices [31–35]. The adsorption of gas molecules or chemicals can physically passivate defects and electrically dope the Fermi level to neutral, resulting in an enhanced PL quantum yield [36–39]. However, the adsorption naturally suffers from weak stability. Directly healing the lattice by repairing the vacancies seems more promising, as it addresses the problem at its root. Calculations suggest that the defect states can also be repaired by filling vacancies with oxygen atoms instead of chalcogenide atoms, making this solution more practical [40]. Thus, chemical treatments including chalcogenide and oxygen annealing, oxygen-incorporated chemical vapor deposition growth, and oxygen plasma treatment have been developed to achieve significant improvements in the performance of TMD-based devices [37,41–45]. However, these drastic treatments also risk breaking the weak covalent bonds, potentially introducing new defects. An ideal strategy should involve a mild lattice repair approach to fully fill the vacancies.

Here, we propose a solid substrate coupling method to eliminate the defect states in mechanically exfoliated WSe_2 samples. By coupling a WSe_2 monolayer with a c-plane sapphire surface, we observed complete suppression of defect-relevant PL peaks and enhanced exciton radiation at cryogenic temperatures. All the experimental results and density functional theory (DFT) calculations indicate that the elimination of the defect-relevant PL peak arises from the repair of selenium vacancies by oxygen atoms from the active c-plane sapphire substrate.

In our experiments, monolayer WSe_2 samples were mechanically exfoliated onto preannealed substrates of c-plane sapphire, a-plane sapphire, and SiO_2/Si (see Supplemental Material Fig. S1 [46]). Under 532 nm laser normal irradiation, the PL spectra of WSe_2 samples were excited and collected in a reflective geometry [Fig. 1(a)]. At room temperature, the spectra exhibited relatively broad peaks located at 1.65 eV, as expected [Fig. 1(b)]. However, the PL intensities of the samples varied with the plane of the sapphire. WSe_2 on c-plane sapphire exhibited a two- to three-fold brighter PL compared to that on a-plane sapphire. This observation was consistent across all samples in our experiment (Supplemental Material [46] Fig. S2) and

strongly indicated an enhanced quantum efficiency for WSe_2 onto c-plane sapphire.

To fully understand this quantum efficiency enhancement, we conducted time-resolved PL spectroscopy and transient PL mapping to monitor the exciton lifetime and diffusion dynamics. The time-resolved PL spectra of monolayer WSe_2 on c-plane and a-plane sapphire substrates are shown in Fig. 1(c). A substantially prolonged PL lifetime was observed, with 420 ps for c-plane sapphire and 170 ps for a-plane, respectively. Furthermore, the diffusion mappings of monolayer WSe_2 on a-plane and c-plane sapphire substrates clearly illustrate the broadening of the PL distribution following excitation [Figs. 1(d) and 1(e)] [47,48]. The exciton diffusivity (D) can be determined via the formula $D = \Delta\sigma^2/2t = (\sigma_t^2 - \sigma_0^2)/2t$, where σ_t^2 represents the mean squared distribution of the PL (the width at half maximum of the PL spatial distribution) at a time delay of t, and σ_0^2 denotes the initial mean squared distribution at $t = 0$. By extracting $\Delta\sigma^2$ from the PL distribution, the diffusivities were determined to be 1.66 ± 0.08 and 1.29 ± 0.07 $cm^2\ s^{-1}$ for WSe_2 on the c-plane and a-plane sapphire substrates, respectively [Fig. 1(f)], suggesting that excitons in WSe_2 on the c-plane sapphire hold a weak scattering effect during diffusion. The enhanced quantum efficiency, together with the prolonged PL lifetime and increased exciton diffusivity, indicates the suppression of defect-related recombination on the c-plane sapphire.

The interplay between 2D materials and substrates has traditionally been attributed to various potential mechanisms, including electronic hybridization, surface phonons, electronic doping, and chemical doping. In this context, electronic hybridization between substrate materials and 2D materials appears improbable, as the PL peak position and intensity are insensitive to the relative lattice orientation between WSe_2 and sapphire (see Supplemental Material [46] Fig. S3).

To mitigate the surface phonon effect and resolve finer PL features, we measured the temperature-dependent PL spectra of WSe_2 on various substrates [Figs. 2(a) and 2(b)]. As the temperature decreased, a noticeable blueshift of the PL peak was observed, as expected. At sufficiently low temperatures, monolayer WSe_2 on a c-plane sapphire substrate exhibited a singular, intense, and sharply defined peak located at 1.73 eV, corresponding to intrinsic exciton, with a typical full width at half maximum of approximately 13 meV [Fig. 2(a)]. In contrast, WSe_2 samples on an a-plane sapphire substrate showed PL peak splitting, with distinct peaks corresponding to different bound quasiparticles [Fig. 2(b)].

As shown in Fig. 2(c), the PL spectrum of monolayer WSe_2 on SiO_2/Si substrate at 7 K was also obtained as a reference. The exciton peak (X^0), trion peak (X^*), and defect-relevant peak (X^D) were discerned based on their energy disparities (see Supplemental Material [46] Fig. S4) [29]. Through multipeak fitting, we observed that

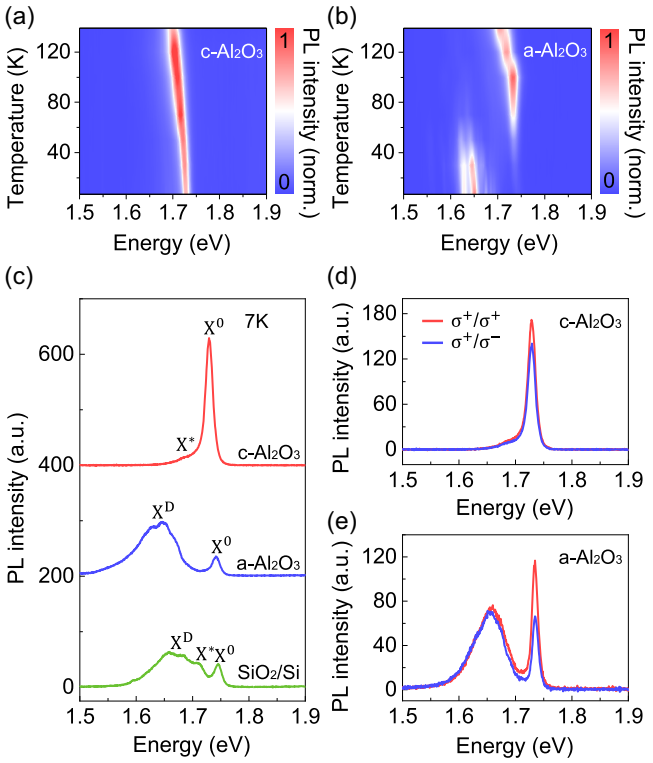

FIG. 2. PL spectra of WSe_2 monolayer at cryogenic temperatures. (a), (b) Temperature-dependent PL spectra of the WSe_2 monolayer on c-plane (a) and a-plane (b) sapphire substrates. As the temperature decreases from 298 to 7 K, the PL peak maintains a singular peak for WSe_2 on c-plane sapphire, but splits into multiple exciton complexes for a-plane sapphire. (c) PL spectra of WSe_2 on different substrates at 7 K. The emission peaks observed on SiO_2/Si substrates correspond precisely to the recombination processes of the neutral exciton (X^0), trion (X^*), and defect-relevant exciton (X^D), respectively. The profile of the WSe_2 sample on a-plane sapphire is similar to that on SiO_2/Si substrate. The monolayer WSe_2 on a c-plane sapphire exhibits a singular, intense, and sharply defined X^0 peak. (d), (e) Valley-polarized PL spectra of WSe_2. Compared with that on a-plane sapphire (e), WSe_2 on c-plane sapphire (d) exhibited smaller valley polarization.

monolayer WSe_2 on the a-plane sapphire substrate exhibited similar PL behavior to that on an SiO_2/Si substrate. However, on the c-plane sapphire, the defect-relevant peaks completely vanished. If we further transfer the monolayer from c-plane to a-plane, no discernible defect peaks are observed either (see Supplemental Material [46] Fig. S5). Additionally, valley-polarized PL spectra were collected, as shown in Figs. 2(d) and 2(e). The PL on c-plane sapphire showed distinct and nearly vanished valley polarization even for an intrinsic neutral exciton [Fig. 2(d)], while samples on a-plane sapphire had a higher degree [Fig. 2(e)]. This is because the valley polarization is determined by the exciton lifetime and depolarization lifetime [49]. At cryogenic temperatures, fewer defects lead to higher exciton

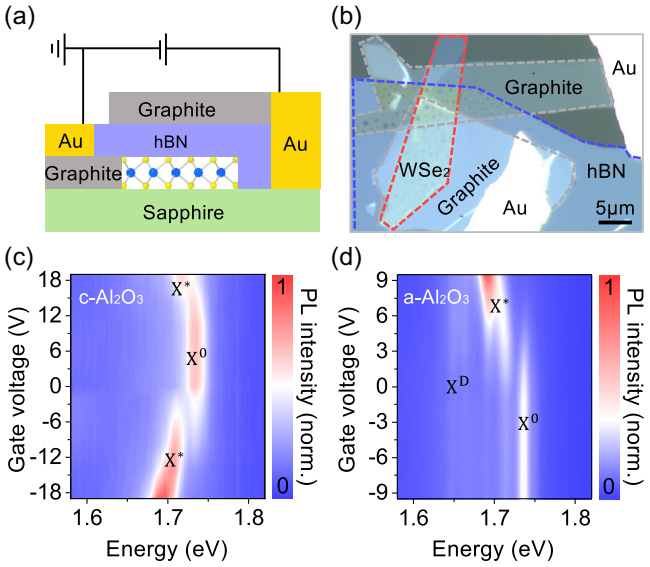

FIG. 3. Doping-dependent PL spectra of WSe_2 monolayer at 7 K. (a), (b) Schematic diagram (a) and optical image (b) of the monolayer WSe_2 device on sapphire substrate. A fragment of graphite served as the contact electrode for the WSe_2, whereas a distinct few-layer graphene was utilized as the transparent top-gate electrode on the top dielectric layer of BN. (c), (d) PL intensity maps as a function of the gate voltage on c-plane (c) and a-plane (d) sapphire. The peaks of X^0, X^*, and X^D are located at 1.73, 1.71, and 1.66 eV, respectively. No defect PL peak appeared regardless of whether a positive or negative voltage was applied for WSe_2 on c-plane sapphire. Nevertheless, the defects were not mitigated by doping WSe_2 on a-plane sapphire.

lifetime and smaller valley polarization (see Supplemental Material (f) for a detailed discussion [46]).

The defect-relevant exciton in WSe_2 has been extensively investigated in previous studies [24–27]. However, the disappearance of defect-relevant PL peaks has never been reported, to the best of our knowledge. In energy space, the defect level resides within the band gap, between the conduction and valence bands. The defect-relevant exciton consists of an electron occupying the defect level and a hole in the valence band. This scenario includes the possibility that substrate-induced electronic doping may raise the Fermi level across the defect states, leading to the disappearance of the defect PL peak.

To address this potential issue, we fabricated devices on sapphire substrates for doping-dependent PL measurements. Top gate devices with hBN as the dielectric layer and graphite as the electrode layer were assembled with WSe_2 monolayers on both the c-plane and a-plane sapphire [Figs. 3(a) and 3(b)]. By adjusting the gate voltage to modulate the carrier density, we systematically investigated the doping-dependent PL spectra. Regardless of whether a positive or negative gate voltage was applied, no discernible defect peaks were present in the monolayer WSe_2 PL spectra on the c-plane sapphire [Fig. 3(c)]. In contrast, for WSe_2 on an a-plane sapphire, the defect PL peak was highly sensitive to doping [Fig. 3(d)]. The intensity decreased with the reduction of applied voltage from positive to negative. However, it consistently appeared within all the spectra (see Supplemental Material [46] Fig. S6). Therefore, it appears that substrate-induced doping does not contribute to the disappearance of the defect PL peak of WSe_2 on c-plane sapphire.

Another likely mechanism is chemical doping. To verify its possibility, we reported DFT calculations of the WSe_2/sapphire system with the Heyd-Scuseria-Ernzerhof exchange-correlation functional and spin-orbit coupling [50]. Figure 4(a) shows the atomic structures of pristine WSe_2, WSe_2 with selenium vacancies (V_{Se}-WSe_2), and oxygen-substituted selenium-site WSe_2 (O_{Se}-WSe_2). The total density of states (TDOS) for these systems are shown in Fig. 4(b). The Se vacancy states are mainly composed of d and p orbitals from W and Se atoms, respectively (see Supplemental Material [46] Fig. S7). When the Se vacancy is filled with an oxygen atom (O_{Se}-WSe_2), the defect states are eliminated, as shown in Fig. 4(b). This is consistent with our experimental observation of the disappearance of defect-related PL peaks.

In the following, we systematically examined the thermodynamic origin of forming O_{Se}-WSe_2 by DFT calculations. The calculations were performed with stable surface structures of both the c-plane and a-plane of Al_2O_3 [51]. We calculated the total energy change (ΔE) of oxygen atom transfer from the Al_2O_3 surface to the selenium vacancy in WSe_2 [Fig. 4(c)]:

$$\Delta E = [E_{WSe_2}(O_{Se}) + E_{Al_2O_3}(V_O)] - [E_{WSe_2}(V_{Se}) + E_{Al_2O_3}],$$

where $E_{WSe_2}(O_{Se})$ is the energy of WSe_2 with one oxygen substitution at the Se site, $E_{Al_2O_3}(V_O)$ is the energy of Al_2O_3 with one oxygen vacancy, $E_{WSe_2}(V_{Se})$ is the energy of WSe_2 with one selenium vacancy, and $E_{Al_2O_3}$ is the energy of the pristine Al_2O_3 with no defects. The results show that the transfer of an oxygen atom from c-Al_2O_3 has a clear thermodynamic advantage over that from a-Al_2O_3. The total energy of the $WSe_2/c-Al_2O_3$ system is significantly reduced after oxygen transfer, explaining the thermodynamic preference of defect repairing by c-Al_2O_3. This tendency is further supported by the pronounced surface reconstruction observed in c-Al_2O_3 after removal of an oxygen atom (see Supplemental Material [46] Fig. S8). The large thermodynamic driving force not only enables barrier-free healing of Se vacancies at the bottom surface of WSe_2, but also facilitates healing of top-surface Se vacancies by overcoming the migration barrier of the

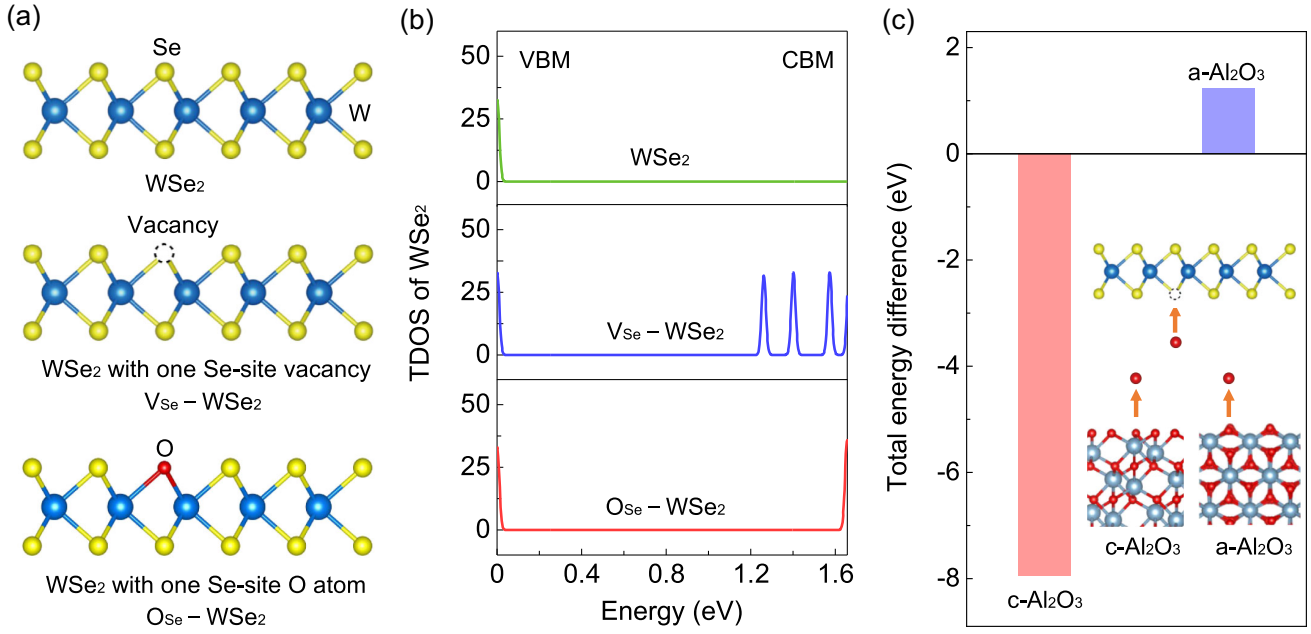

FIG. 4. DFT calculations of defect eliminating in WSe_2 monolayer. (a) Side view of WSe_2 monolayer. Tungsten atoms are shown in blue, selenium atoms are shown in yellow, and oxygen atoms are shown in red. From top to bottom: pristine WSe_2 (WSe_2),WSe_2 with one selenium vacancy (V_{Se}-WSe_2) and WSe_2 with an oxygen atom at the selenium site (O_{Se}-WSe_2). (b) TDOS of the $4 \times 4 \times 1$ supercell WSe_2 monolayer corresponding to (a). (c) Total energy difference after a single oxygen atom transfers from the Al_2O_3 surface to the selenium vacancy in WSe_2 monolayer. A negative value indicates a preference for the oxygen atom to transfer to the selenium vacancy.

Se atom across the WSe_2 layer (see Supplemental Material [46] Fig. S9).

In summary, our Letter demonstrates that the mechanically exfoliated WSe_2 monolayer exhibits intrinsic and bright neutral-exciton PL emission at cryogenic temperatures when coupled with c-plane sapphire. Further experiments and *ab initio* calculations suggest that this defect elimination effect is likely attributed to the selenium vacancies being repaired by the highly active oxygen-terminated c-plane sapphire. This Letter paves the way for eliminating defect states in 2D monolayers through interfacial coupling, thereby improving physical properties such as electrical conductivity, mechanical strength, and thermal performance.

Acknowledgments—This work is supported by the National Natural Science Foundation of China (Grants No. 12422406, No. 12404208, No. 52025023, and No. 12374167), National Key R&D Program of China (Grants No. 2021YFA1400200 and No. 2022YFA1403500), Guangdong Major Project of Basic and Applied Basic Research (Grant No. 2021B0301030002), and the New Cornerstone Science Foundation through the XPLORER PRIZE.

Data availability—The data that support the findings of this Letter are not publicly available upon publication because it is not technically feasible and/or the cost of preparing, depositing, and hosting the data would be prohibitive within the terms of this research project. The data are available from the authors upon reasonable request.

[1] G. Wang, A. Chernikov, M. M. Glazov, T. F. Heinz, X. Marie, T. Amand, and B. Urbaszek, Colloquium: Excitons in atomically thin transition metal dichalcogenides, Rev. Mod. Phys. **90**, 021001 (2018).
[2] N. P. Wilson, W. Yao, J. Shan, and X. D. Xu, Excitons and emergent quantum phenomena in stacked 2D semiconductors, Nature (London) **599**, 383 (2021).
[3] E. C. Regan *et al.*, Emerging exciton physics in transition metal dichalcogenide heterobilayers, Nat. Rev. Mater. **7**, 778 (2022).
[4] D. Y. Qiu, F. H. Da Jornada, and S. G. Louie, Optical spectrum of MoS_2: Many-body effects and diversity of exciton states, Phys. Rev. Lett. **111**, 216805 (2013).
[5] K. F. Mak *et al.*, Tightly bound trions in monolayer MoS_2, Nat. Mater. **12**, 207 (2013).
[6] J. S. Ross *et al.*, Electrical control of neutral and charged excitons in a monolayer semiconductor, Nat. Commun. **4**, 1474 (2013).
[7] X. D. Xu, W. Yao, D. Xiao, and T. F. Heinz, Spin and pseudospins in layered transition metal dichalcogenides, Nat. Phys. **10**, 343 (2014).
[8] M. R. Molas *et al.*, Brightening of dark excitons in monolayers of semiconducting transition metal dichalcogenides, 2D Mater. **4**, 021003 (2017).

[9] X. X. Zhang *et al.*, Magnetic brightening and control of dark excitons in monolayer WSe_2, Nat. Nanotechnol. **12**, 883 (2017).
[10] G. Wang *et al.*, In-plane propagation of light in transition metal dichalcogenide monolayers: Optical selection rules, Phys. Rev. Lett. **119**, 047401 (2017).
[11] Y. Zhou *et al.*, Probing dark excitons in atomically thin semiconductors via near-field coupling to surface plasmon polaritons, Nat. Nanotechnol. **12**, 856 (2017).
[12] S. Y. Chen, T. Goldstein, T. Taniguchi, K. Watanabe, and J. Yan, Coulomb-bound four- and five-particle intervalley states in an atomically-thin semiconductor, Nat. Commun. 2018) 3717 ,**9**).
[13] Z. P. Li *et al.*, Revealing the biexciton and trion-exciton complexes in BN encapsulated WSe_2, Nat. Commun. **9**, 3719 (2018).
[14] M. Barbone *et al.*, Charge-tuneable biexciton complexes in monolayer WSe_2, Nat. Commun. **9**, 3721 (2018).
[15] A. V. Stier, N. P. Wilson, K. A. Velizhanin, J. Kono, X. Xu, and S. A. Crooker, Magnetooptics of exciton rydberg states in a monolayer semiconductor, Phys. Rev. Lett. **120**, 057405 (2018).
[16] Z. L. Ye *et al.*, Efficient generation of neutral and charged biexcitons in encapsulated WSe_2 monolayers, Nat. Commun. **9**, 3718 (2018).
[17] Z. P. Li *et al.*, Momentum-dark intervalley exciton in monolayer tungsten diselenide brightened via chiral phonon, ACS Nano **13**, 14107 (2019).
[18] Z. P. Li *et al.*, Emerging photoluminescence from the dark-exciton phonon replica in monolayer WSe_2, Nat. Commun. **10**, 2469 (2019).
[19] Z. P. Li, J. vanBaren, Z. Lu, M. M. Altaiary, T. Taniguchi, K. Watanabe, D. Smirnov, and C. H. Lui, Direct observation of gate-tunable dark trions in monolayer WSe_2, Nano Lett. **19**, 6886 (2019).
[20] E. Liu *et al.*, Gate tunable dark trions in monolayer WSe_2, Phys. Rev. Lett. **123**, 027401 (2019).
[21] M. R. Molas *et al.*, Probing and manipulating valley coherence of dark excitons in monolayer WSe_2, Phys. Rev. Lett. **123**, 096803 (2019).
[22] R. J. Gelly *et al.*, Probing dark exciton navigation through a local strain landscape in a WSe_2 monolayer, Nat. Commun. **13**, 232 (2022).
[23] H. N. Wang, C. J. Zhang, and F. Rana, Ultrafast dynamics of defect-assisted electron hole recombination in monolayer MoS_2, Nano Lett. **15**, 339 (2015).
[24] S. Zhang, C. G. Wang, M. Y. Li, D. Huang, L. J. Li, W. Ji, and S. Wu, Defect structure of localized excitons in a WSe_2 monolayer, Phys. Rev. Lett. **119**, 046101 (2017).
[25] G. Moody, K. Tran, X. Lu, T. Autry, J. M. Fraser, R. P. Mirin, L. Yang, X. Li, and K. L. Silverman, Microsecond valley lifetime of defect-bound excitons in monolayer WSe_2, Phys. Rev. Lett. **121**, 057403 (2018).
[26] S. Refaely-Abramson, D. Y. Qiu, S. G. Louie, and J. B. Neaton, Defect-induced modification of low-lying excitons and valley selectivity in monolayer transition metal dichalcogenides, Phys. Rev. Lett. **121**, 167402 (2018).
[27] Y. J. Zheng *et al.*, Point defects and localized excitons in 2D WSe_2, ACS Nano **13**, 6050 (2019).
[28] K. Greben, S. Arora, M. G. Harats, and K. Bolotin, Intrinsic and extrinsic defect-related excitons in TMDCs, Nano Lett. **20**, 2544 (2020).
[29] E. Lorchat *et al.*, Filtering the photoluminescence spectra of atomically thin semiconductors with grapheme, Nat. Nanotechnol. **15**, 283 (2020).
[30] P. Rivera *et al.*, Intrinsic donor-bound excitons in ultraclean monolayer semiconductors, Nat. Commun. **12**, 871 (2021).
[31] Z. H. Hu, Z. T. Wu, C. Han, J. He, Z. H. Ni, and W. Chen, Two-dimensional transition metal dichalcogenides: Interface and defect engineering, Chem. Soc. Rev. **47**, 3100 (2018).
[32] D. Edelberg *et al.*, Approaching the intrinsic limit in transition metal diselenides via point defect control, Nano Lett. **19**, 4371 (2019).
[33] M. F. Zhou, W. H. Wang, J. P. Lu, and Z. H. Ni, How defects influence the photoluminescence of TMDCs, Nano Res. **14**, 29 (2021).
[34] S. Y. Seo *et al.*, Reconfigurable photo-induced doping of two-dimensional van der Waals semiconductors using different photon energies, Nat. Electron. **4**, 38 (2021).
[35] Q. H. Tan *et al.*, Layer-dependent correlated phases in WSe_2/MoS_2 moire superlattice, Nat. Mater. **22**, 605 (2023).
[36] S. Tongay *et al.*, Broad-range modulation of light emission in two-dimensional semiconductors by molecular physisorption gating, Nano Lett. **13**, 2831 (2013).
[37] H. Y. Nan *et al.*, Strong photoluminescence enhancement of MoS_2 through defect engineering and oxygen bonding, ACS Nano **8**, 5738 (2014).
[38] M. Amani *et al.*, Near-unity photoluminescence quantum yield in MoS_2, Science **350**, 1065 (2015).
[39] D. H. Lien *et al.*, Electrical suppression of all nonradiative recombination pathways in monolayer semiconductors, Science **364**, 468 (2019).
[40] J. P. Lu *et al.*, Atomic healing of defects in transition metal dichalcogenides, Nano Lett. **15**, 3524 (2015).
[41] M. R. Islam *et al.*, Tuning the electrical property defect engineering of single layer MoS_2 by oxygen plasma, Nanoscale **6**, 10033 (2014).
[42] W. S. Leong, Y. Li, X. Luo, C. T. Nai, S. Y. Quek, and J. T. L. Thong, Tuning the threshold voltage of MoS_2 field-effect transistors surface treatment, Nanoscale **7**, 10823 (2015).
[43] M. S. Kim *et al.*, Photoluminescence wavelength variation of monolayer MoS_2 by oxygen plasma treatment, Thin Solid Films **590**, 318 (2015).
[44] W. Zhao, J. Ma, P. Sun, K. L. Zhang, and Y. J. Yuan, Strong photoluminescence enhancement of MoS_2 monolayer via low-power Ar/O plasma treatment, Mater. Lett. **235**, 129 (2019).
[45] P. C. Shen *et al.*, Healing of donor defect states in monolayer molybdenum disulfide using oxygen-incorporated chemical vapour deposition, Nat. Electron. **5**, 28 (2022).
[46] See Supplemental Material at http://link.aps.org/supplemental/10.1103/lswx-rxss for additional experiment details.
[47] H. Liu, C. Wang, Z. G. Zuo, D. M. Liu, and J. B. Luo, Direct visualization of exciton transport in defective few-layer WS_2 by ultrafast microscopy, Adv. Mater. **32**, 1906540 (2020).

[48] S. B. Deng, E. Z. Shi, L. Yuan, L. R. Jin, L. T. Dou, and L. B. Huang, Long-range exciton transport and slow annihilation in two-dimensional hybrid perovskites, Nat. Commun. **11**, 664 (2020).

[49] A. M. Jones *et al.*, Optical generation of excitonic valley coherence in monolayer WSe_2, Nat. Nanotechnol. **8**, 634 (2013).

[50] A. V. Krukau, O. A. Vydrov, A. F. Izmaylov, and G. E. Scuseria, Influence of the exchange screening parameter on the performance of screened hybrid functional, J. Chem. Phys. **125**, 224106 (2006).

[51] T. Kurita, K. Uchida, and A. Oshiyama, Atomic and electronic structures of $\alpha - Al_2O_3$ surfaces, Phys. Rev. B **82**, 155319 (2010).